




Article

# Nanocomposites SnO<sub>2</sub>/SiO<sub>2</sub> for CO Gas Sensors: Microstructure and Reactivity in the Interaction with the Gas Phase

Dayana Gulevich <sup>1</sup>, Marina Rumyantseva <sup>1,\*</sup> , Evgeny Gerasimov <sup>2</sup> , Artem Marikutsa <sup>1</sup> , Valeriy Krivetskiy <sup>1</sup>, Tatyana Shatalova <sup>1</sup>, Nikolay Khmelevsky <sup>3</sup> and Alexander Gaskov <sup>1</sup>

<sup>1</sup> Chemistry Department, Moscow State University, 119991 Moscow, Russia; dayana-nsu@mail.ru (D.G.); artem.marikutsa@gmail.com (A.M.); vkrivetskiy@gmail.com (V.K.); shatalovtb@gmail.com (T.S.); gaskov@inorg.chem.msu.ru (A.G.)

<sup>2</sup> Boreskov Institute of Catalysis SB RAS, 630090 Novosibirsk, Russia; gerasimov@catalysis.ru

<sup>3</sup> LISM, Moscow State Technological University Stankin, 127055 Moscow, Russia; khmelevsky@mail.ru

\* Correspondence: room@inorg.chem.msu.ru; Tel.: +7-495-939-5471

Received: 15 March 2019; Accepted: 29 March 2019; Published: 2 April 2019



**Abstract:** Nanocomposites SnO<sub>2</sub>/SiO<sub>2</sub> with a silicon content of [Si]/([Sn] + [Si]) = 3/86 mol.% were obtained by the hydrothermal method. The composition and microstructure of the samples were characterized by EDX, XRD, HRTEM and single-point Brunauer-Emmet-Teller (BET) methods. The surface sites were investigated using thermal analysis, FTIR and XPS. It is shown that the insertion of silicon dioxide up to the value of [Si]/([Sn] + [Si]) = 19 mol.% stabilizes the growth of SnO<sub>2</sub> nanoparticles during high-temperature annealing, which makes it possible to obtain sensor materials operating stably at different temperature conditions. The sensor properties of SnO<sub>2</sub> and SnO<sub>2</sub>/SiO<sub>2</sub> nanocomposites were studied by in situ conductivity measurements in the presence of 10–200 ppm CO in dry and humid air in the temperature range of 150–400 °C. It was found that SnO<sub>2</sub>/SiO<sub>2</sub> nanocomposites are more sensitive to CO in humid air as compared to pure SnO<sub>2</sub>, and the sample with silicon content [Si]/([Sn] + [Si]) = 13 mol.% is resistant to changes in relative air humidity (RH = 4%–65%) in the whole temperature range, which makes it a promising sensor material for detecting CO in real conditions. The results are discussed in terms of the changes in the composition of surface-active groups, which alters the reactivity of the obtained materials.

**Keywords:** nanocomposites; tin dioxide; silicon dioxide; hydrothermal synthesis; gas sensor; carbon monoxide; humidity; active surface groups

## 1. Introduction

Due to their physicochemical properties, wide-gap semiconductor metal oxides, such as SnO<sub>2</sub>, ZnO, WO<sub>3</sub>, In<sub>2</sub>O<sub>3</sub>, are widely used as materials for resistive-type gas sensors. Among them, tin dioxide has the greatest practical application. SnO<sub>2</sub> is a wide-gap n-type semiconductor ( $E_g = 3.6$  eV at 300 K [1]) which is effectively used to detect toxicity reducing gases CO, H<sub>2</sub>S, NH<sub>3</sub>, as well as volatile organic compounds (VOCs). The main requirements for the sensor material are selectivity, high sensitivity and thermal stability. The latter property is extremely important for the long-term operation of the sensor, as well as for measurements in a dynamic temperature mode (frequently used in e-nose devices), which allows an increase of the sensor signal due to more effective desorption of the products of the redox reaction from the surface of the semiconductor oxide [2–5]. In order to avoid sintering the nanoparticles of the sensor material when operating in such temperature conditions, it is necessary to carry out post-synthetic annealing at a temperature exceeding the expected maximum operating temperature during sensor functioning. However, the specific surface area of inorganic

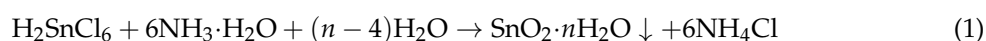
materials decreases by ~30%–40% with an increase in heat treatment temperature for every 100 °C [6,7]. It is possible to prevent aggregation and the sintering of nanoparticles by synthesizing SnO<sub>2</sub> in a polymer matrix, or using surfactants [8,9], as well as with the addition of metal oxides (Mn, Mg, Co, Ni, Zn, Ca, Ba, V, Cu, etc.) and non-metals (P, B, S). A uniform distribution of such modifiers over tin dioxide surface reduces the surface energy at SnO<sub>2</sub> grain boundaries and prevent the growth of particles during heat treatment [10–12]. However, the introduction of the second component inevitably leads to a change in the type and concentration of active centers on the surface of SnO<sub>2</sub>, which affects the sensor properties. To reduce the likelihood of side reactions, it is preferable to select a modifier with low own catalytic activity. This requirement is met by amorphous SiO<sub>2</sub>, which is also characterized by high thermal stability (Tamman temperature is 714 °C) [13]. In a number of studies on the synthesis of SnO<sub>2</sub>/SiO<sub>2</sub> composites of various morphologies, a decrease in the growth rate and stabilization of SnO<sub>2</sub> microstructure parameters, as well as an increase in the sensor signal to acetone, ethanol, and CO in dry and moist air were observed [14–21]. The decisive factor in the synthesis of such composites is the selection of the optimal Si:Sn ratio. Since silicon dioxide is a dielectric, its excessive content can lead to a disruption of the intergranular conductivity of SnO<sub>2</sub>.

The aims of this work were to synthesize SnO<sub>2</sub>/SiO<sub>2</sub> nanocomposites that are resistant to sintering during long-term high-temperature annealing, to determine the Si:Sn ratio optimal for sensor measurements, to study the effect of silicon dioxide on the microstructure parameters and the active sites on the tin dioxide surface; and, finally, to reveal the influence of these parameters on the sensor properties of SnO<sub>2</sub>/SiO<sub>2</sub> nanocomposites in CO detection in dry and humid air. The latter is of particular interest, since our previous work showed the efficiency of using SiO<sub>2</sub> layer as a passive filter to reduce the negative effect of humidity on the SnO<sub>2</sub> sensor properties toward CO [22].

## 2. Materials and Methods

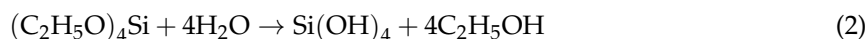
### 2.1. Materials Synthesis

Tin dioxide was obtained as a result of thermal decomposition of  $\alpha$ -stannic acid gel precipitated from H<sub>2</sub>SnCl<sub>6</sub> solution (SnCl<sub>4</sub>·5H<sub>2</sub>O, 98%, Sigma-Aldrich, Saint Louis, MO, USA) using aqueous ammonia:



The ammonia solution was added until reaching pH 6.5–7.0. The obtained  $\alpha$ -stannic acid gel was separated by centrifugation and washed several times from the chloride ions with deionized water until the beginning of the peptization process, then with NH<sub>4</sub>NO<sub>3</sub> (99%, Sigma-Aldrich) solution. After a negative reaction with AgNO<sub>3</sub>, the precipitate was dried at 50 °C for 24 h and the xerogel of  $\beta$ -stannic acid, SnO<sub>2</sub> · xH<sub>2</sub>O, was obtained.

Tetraethoxysilane (TEOS) (98%, Sigma-Aldrich) was used as SiO<sub>2</sub> precursor. At the first stage, the reaction was carried out at 25 °C for 24 h:



The hydrolysis was carried out in a reaction medium consisting of 90% ethyl alcohol, 5% water and 5% TEOS (by volume) with acetic acid added to pH = 4, so that the hydrolysis rate exceeded the polycondensation rate.

To obtain the SnO<sub>2</sub>/SiO<sub>2</sub> composites by the hydrothermal method, the SnO<sub>2</sub> · xH<sub>2</sub>O xerogel and an alcohol solution of Si(OH)<sub>4</sub> were placed in an autoclave at a temperature of 150 °C for 24 h. The reaction was carried out with a constant stirring. The temperature was controlled using a thermocouple in contact with the lid of the autoclave. The reaction product was repeatedly washed with alcohol and water during centrifugation and dried at room temperature. According to the thermal analysis with mass spectral determination of gaseous products (CO<sub>2</sub>, *m/z* = 44; H<sub>2</sub>O, *m/z* = 18), the optimum annealing temperature of the samples was set at 600 °C, since all possible organic by-products of the

TEOS hydrolysis decompose at a temperature of 500–550 °C (Figure 1). The thermal treatment was carried out in air for 24 h. The composition of the samples was pre-assigned as  $[\text{Si}]/([\text{Sn}] + [\text{Si}]) = 3, 13, 19, 49, \text{ and } 86$  mol.% (which will be referred to as SnSi3, SnSi13, SnSi19, SnSi49 and SnSi86 respectively). The designations of samples and their characteristics are given in Table 1.

**Table 1.** Composition, parameters of microstructure and electrophysical properties of the obtained samples.

Sample	$\frac{[\text{Si}]}{[\text{Si}] + [\text{Sn}]}$ mol.% <sup>a</sup>	$d_{\text{XRD}}(\text{SnO}_2)$ , nm <sup>b</sup>	$S_{\text{BET}} \pm 5$ m <sup>2</sup> /g <sup>c</sup>	$R(100\text{ °C})$ , $\Omega$ <sup>d</sup>
SnO <sub>2</sub>	0	11 ± 1	23	$7.3 \times 10^7$
SnSi3	3	8 ± 1	29	$1.5 \times 10^8$
SnSi13	13	7 ± 1	99	$3.2 \times 10^8$
SnSi19	19	6 ± 1	156	$2.2 \times 10^9$
SnSi49	49	9 ± 1	82	$>10^{12}$
SnSi86	86	10 ± 1	22	$>10^{12}$
SiO <sub>2</sub>	100	–	327	insulator

<sup>a</sup>: determined by EDX; <sup>b</sup>: SnO<sub>2</sub> crystallite size; <sup>c</sup>: specific surface area; <sup>d</sup>: resistance in air at 100 °C.

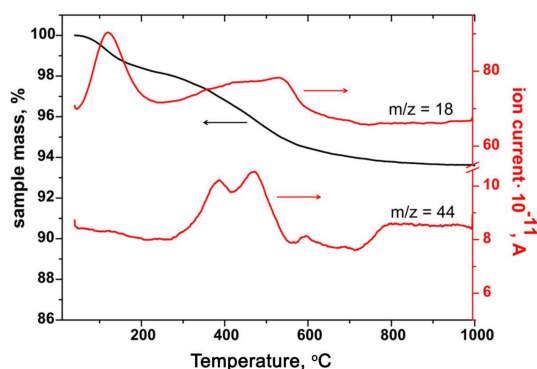


**Figure 1.** Thermogravimetric and mass spectral analysis of the SnSi49 sample before heat treatment.

## 2.2. Materials Characterization

A determination of the temperature of decomposition of the dried products of hydrothermal synthesis was made by thermal analysis with simultaneous registration of gaseous products by the mass spectral method. Thermal analysis of the samples was carried out on an STA 409 HC Luxx thermal analyzer (Netzsch-Gerätebau GmbH, Selb, Germany). Heating was performed in air flow (30 mL/min) at a rate of 10 °C/min. Mass spectral analysis of gaseous products released during the thermal decomposition of the samples was performed using a QMS 403 C Aëolos quadrupole mass spectrometer (Netzsch, Germany).

The composition of the samples was investigated by energy dispersive X-ray spectroscopy (EDX) using Zeiss NVision 40 (Carl Zeiss, Oberkochen, Germany) scanning electron microscope equipped with a X-Max detector (Oxford Instruments, Abington, UK) operated at 20 kV. The phase composition and size of the crystal grains of semiconductor materials were determined by X-ray diffraction on a DRON-4 diffractometer using monochromatic Cu K $\alpha$  radiation ( $\lambda = 1.5406 \text{ \AA}$ ). The survey was carried out in the range of  $2\theta = 10^\circ\text{--}60^\circ$  with a step of  $0.1^\circ$ . The crystallite size  $d_{\text{XRD}}$  of SnO<sub>2</sub> phase was estimated from the broadening of the reflections using the Scherer formula. The phase composition was established using the STOE WinXPOW Version 1.04 program. The determination of specific surface area was performed by low-temperature nitrogen adsorption on ASAP 2020 and Chemisorb 2750 devices (Micromeritics) with subsequent analysis using the BET model.

The microstructure of nanocomposites, as well as of individual SnO<sub>2</sub> and SiO<sub>2</sub> oxides, was studied using high-resolution transmission electron microscopy on a JEM 2010 (JEOL, Tokyo, Japan) instrument

with an accelerating voltage of 200 kV and a lattice resolution of 0.14 nm. The images were recorded using a CCD matrix of the Soft Imaging System (Mega View III, Münster, Germany). The device is equipped with an XFlash energy dispersive X-ray emission spectrometer (EDX) (Bruker, Germany) with a semiconductor Si detector with an energy resolution of 130 eV.

The surface composition was studied using infrared spectroscopy (FTIR, Perkin Elmer Inc., Waltham, MA, USA) and X-ray photoelectron spectroscopy (XPS, Thermo Fisher Scientific, Waltham, MA, USA). The infrared (IR) spectra were recorded on a Frontier FT-IR spectrometer in the transmission mode in the wavenumbers range of 4000–400  $\text{cm}^{-1}$  with 1  $\text{cm}^{-1}$  step. The content of test substances in a KBr tablet (Sigma-Aldrich, “For FTIR analysis”) was 1 wt.%. The X-ray photoelectron spectra were obtained on a K-Alpha (Thermo Scientific, Waltham, MA, USA) spectrometer equipped with a monochromatic Al  $K\alpha$  X-ray source ( $E = 1486.7$  eV). The positions of the peaks in the binding energy scale were corrected using the C1s peak corresponding to the carbon contamination of the surface (285.0 eV) with an accuracy of 0.1 eV. XP-spectra were fitted by Gaussian-Lorentzian convolution functions with simultaneous optimization of Shirley background parameters.

### 2.3. Study of Sensor Properties

For electrophysical and gas sensor measurements the powders of  $\text{SnO}_2$  and  $\text{SnO}_2/\text{SiO}_2$  nanocomposites were mixed with  $\alpha$ -terpeniol (90%, Kosher, SAFC) to form a paste and then deposited on alumina substrates with platinum contacts on the top side and platinum heater on the back side. The resulting thick films were dried at 50 °C for 24 h and annealed at 300 °C to remove residual organic binder.

The sensor properties of the materials towards CO were investigated by in situ measurements of electrical conductivity in a flow cell under controlled gas flow of  $100 \pm 0.1$  mL/min. The measurements were carried out in the temperature interval of 400–150 °C in 50 °C steps, in the range of CO concentrations of 10–200 ppm in air. Attested gas mixture CO ( $0.047 \pm 0.002$  vol.%) /  $\text{N}_2$  was used as a source of carbon monoxide. Purified air was used as a background gas. The creation of gas mixtures with relative humidity (at 25 °C)  $\text{RH} > 1\%$  was carried out by bubbling a part of the gas stream through a vessel with distilled water. The RH value was determined using a humidity measuring device IVTM-7 (Practic-NC, Zelenograd, Russia). The measurements were carried out under conditions of cyclic changes in the gas phase composition (three cycles for each temperature). The duration of measurements in the presence of CO and in pure air was 15 min. The magnitude of the sensor response ( $S$ ) was calculated as  $S = R_{\text{air}}/R_{\text{gas}}$ , where  $R_{\text{air}}$ —resistance of the sample in air, and  $R_{\text{gas}}$ —resistance in the presence of CO.

## 3. Results and Discussion

The composition of  $\text{SnO}_2/\text{SiO}_2$  samples determined by the EDX method is in good agreement with the Si/Sn ratio pre-assigned during the synthesis (Figure 2, Table 1). X-ray diffraction patterns of  $\text{SnO}_2/\text{SiO}_2$  nanocomposites (SnSi3–SnSi86 samples) contain only reflections corresponding to the  $\text{SnO}_2$  phase with a cassiterite structure (ICDD 41-1445). Silicon dioxide obtained by the hydrothermal method is X-ray amorphous (Figure 3). Crystalline phases of tin silicates are not formed under synthesis conditions. When silicon is introduced into nanocomposites, the diffraction reflections of the tin dioxide phase are broadened, which indicates a decrease in the size of the  $\text{SnO}_2$  crystal grains. Under isothermal annealing, the presence of impurities on the surface of growing crystallites slows down their growth rate due to the so-called Smith-Zener diffusion drag [23], according to which the maximum crystal grain size is determined by the volume fraction and particle size of another phase (including amorphous) segregated on the surface growing crystallites.

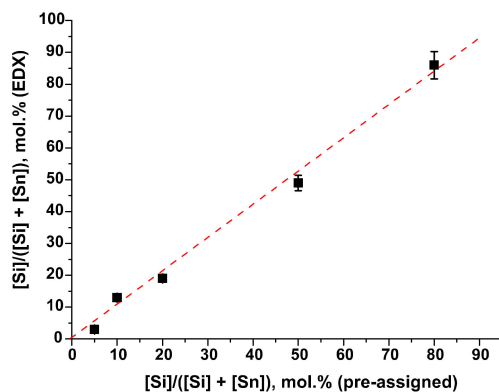


**Figure 2.** Correlation between silicon content in SnO<sub>2</sub>/SiO<sub>2</sub> nanocomposites determined by EDX and pre-assigned during the synthesis.

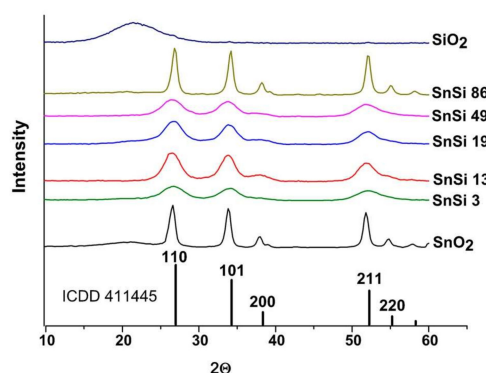


**Figure 3.** XRD patterns of nanocrystalline SnO<sub>2</sub>, SiO<sub>2</sub> and SnO<sub>2</sub>/SiO<sub>2</sub> nanocomposites. Vertical lines correspond to the ICDD 41-1445 reference (SnO<sub>2</sub> cassiterite).

Since the key stages in the interaction of the sensor material with the gas being determined are adsorption and redox reactions on the surface of the semiconductor oxide, the high value of the specific surface area is the most important characteristic of the sample. With an increase in the annealing temperature from 300 to 600 °C, the specific surface area of SnO<sub>2</sub> decreases from 90–100 to 15–20 m<sup>2</sup>/g, respectively [24]. At the same time a high annealing temperature allows one to obtain thermally stable sensor materials for which long-term measurements don't lead to sintering and coarsening of nanoparticles. The tendency to a sharp decrease in the specific surface area of pure SnO<sub>2</sub> is also retained in the case of hydrothermal treatment of the oxide before annealing.

From the SnO<sub>2</sub> crystallite size calculated by Sherer formula it can be concluded that the addition of SiO<sub>2</sub> reduces the growth rate of tin dioxide nanocrystals at high annealing temperature. With the growth of silicon content in SnO<sub>2</sub>/SiO<sub>2</sub> composites up to [Si]/([Sn] + [Si]) = 19 mol.%, an increase in the specific surface area is observed. With a further increase in [Si]/([Sn] + [Si]) ratio to 49 and 86 mol.% specific surface area of nanocomposites decreases sharply and in the latter case is almost equal to the value obtained for pure SnO<sub>2</sub> (Figure 4). The N<sub>2</sub> adsorption-desorption curves for pure SnO<sub>2</sub> (Figure 5a) and SnSi19 nanocomposite (Figure 5b) can be attributed to type V and type IV, respectively. In both cases the hysteresis is observed, that indicates the irreversible capillary condensation. According to the IUPAC classification, in the case of SnO<sub>2</sub>, the hysteresis is of the H1 type, which is characteristic of a porous, spatially ordered structure that has minimal connectivity between adjacent pores. The hysteresis of the N<sub>2</sub> adsorption-desorption curve of the SnSi19 nanocomposite is of the H2a type that indicates a more complex structure of mesopores characteristic for silica gels.

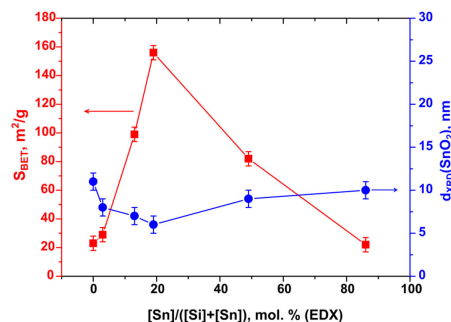


**Figure 4.** Specific surface area  $S_{BET}$  and  $SnO_2$  crystallite size  $d_{XRD}$  depending on silicon content in  $SnO_2/SiO_2$  nanocomposites annealed at 600 °C.

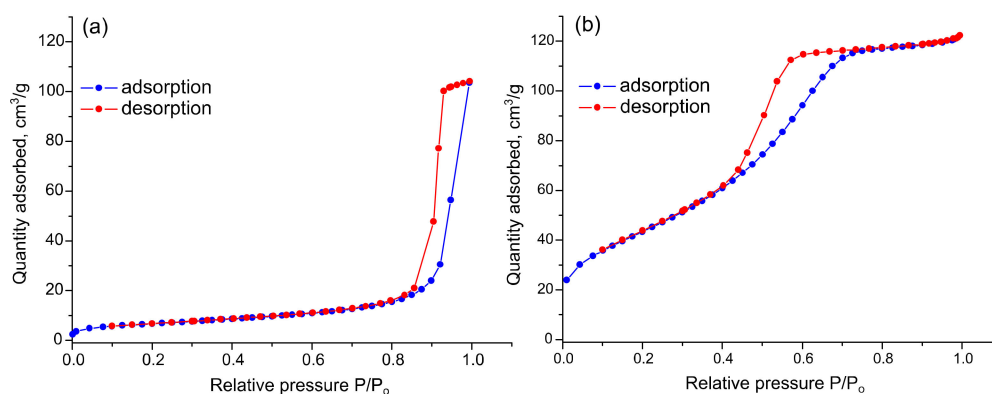


**Figure 5.**  $N_2$  adsorption and desorption curves of nanocrystalline  $SnO_2$  (a) and  $SnSi19$  nanocomposite (b).

To explain the observed dependence of microstructure parameters on the composition of  $SnO_2/SiO_2$  nanocomposites, we consider the process of nucleation of  $SiO_2$  on the surface of a previously formed solid phase of  $\beta$ -stannic acid. According to the classical nucleation theory, the work of heterogeneous nucleation is always less than the work of the formation of nuclei of a new phase through a homogeneous mechanism. Consequently, the nucleation becomes possible at low supersaturations. Thus, in the range of  $[Si]/([Sn] + [Si]) = 3\text{--}19$  mol.%, the concentration of Si(IV) in the reaction medium is low and the supersaturation required for the formation of  $SiO_2$  nuclei in the volume of the reaction mixture is not reached. As a result, in the process of hydrothermal treatment  $SiO_2$  is formed by the mechanism of heterogeneous nucleation on the surface of  $SnO_2$  nanoparticles thus preventing their coarsening during subsequent heat treatment. With an increase in the concentration of silica precursor in the synthesis of  $SnSi49$  and  $SnSi86$  samples, the supersaturation necessary for homogeneous formation of  $SiO_2$  nuclei in the volume of the reaction mixture seems to be achieved. Thus, the number of  $SiO_2$  nuclei, covering the surface of  $SnO_2$ , nanoparticles decreases. As a result, there is a sharp decrease in the value of the specific surface area for the nanocomposites with  $[Si]/([Sn] + [Si]) > 19$  mol.%. The specific surface area of pure  $SiO_2$  obtained by the hydrothermal method from hydrolyzed tetraethoxysilan was  $327 \pm 5$   $m^2/g$ . Thus, the sintering of  $SnO_2$  nanoparticles is responsible for reducing the specific surface area of nanocomposites. Formation of  $SiO_2$  fragments on the surface of tin dioxide grains by heterogeneous nucleation successfully withstands this process.

According to the HREM image of unmodified  $SnO_2$  (Figure 6a), it can be concluded that tin dioxide consists mainly of large crystalline nanoparticles, while  $SiO_2$  is completely amorphous (Figure 6d). On the images of  $SnSi13$  and  $SnSi49$  samples (Figure 6b,c) one can easily highlight the crystalline phase of  $SnO_2$  and amorphous silica particles which are distributed fairly evenly on the surface of the semiconductor oxide. Separate large  $SiO_2$  aggregates are not observed even for the  $SnSi49$  sample. The size of the crystalline particles in the composite samples decreases as compared to pure  $SnO_2$  and the proportion of the amorphous silica phase increases from  $SnSi13$  to  $SnSi49$ . With an increase in the silicon concentration, the resistance of nanocomposites grows greatly due to an increase in the

fraction of the dielectric SiO<sub>2</sub> (Table 1). The resistance values for SnSi49 and SnSi86 samples exceed 10<sup>11</sup> Ohm even at high temperature (400 °C), which makes them unsuitable for use as sensor materials.

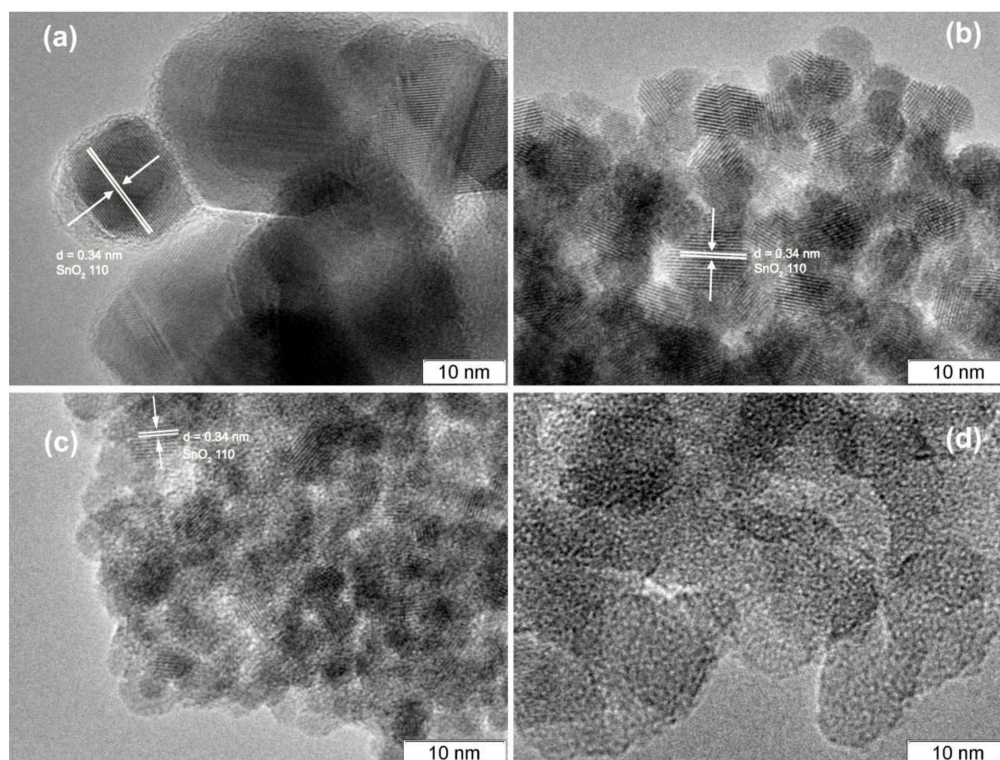
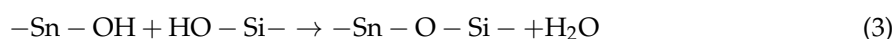


**Figure 6.** HREM images of: (a) SnO<sub>2</sub>; (b) SnSi13; (c) SnSi49; (d) SiO<sub>2</sub>.

FTIR spectroscopy was used to investigate how the introduction of silicon dioxide affects the composition of active groups on SnO<sub>2</sub> surface. The IR of unmodified tin dioxide (Figure 7a) contains stretching vibrations of O–H groups (3650–2500 cm<sup>−1</sup>), physically adsorbed water (1635 cm<sup>−1</sup>), antisymmetric vibrations of Sn–O–Sn bridge groups (670 cm<sup>−1</sup>), terminal Sn–OH bonds (590 cm<sup>−1</sup>) and symmetric vibrations of Sn–O (530 cm<sup>−1</sup>) [25]. On the IR spectrum of pure SiO<sub>2</sub> (Figure 7a), the oscillations of hydroxyl groups and adsorbed H<sub>2</sub>O are practically absent. The broad absorption band with a maximum at 1100 cm<sup>−1</sup> is due to the superposition of antisymmetric vibrations of Si–O–Si bridge bonds and vibrations of silanol groups (1250–870 cm<sup>−1</sup>). The spectrum also contains absorption bands corresponding to the symmetric vibrations of Si–O–Si (810 cm<sup>−1</sup>) and to the deformation vibrations of Si–O (460 cm<sup>−1</sup>) [26]. To estimate the change in the concentration of surface groups, the IR spectra of the composite samples were normalized to the intensity of Sn–O–Sn oscillation (670 cm<sup>−1</sup>) (Figure 7b,c). As the [Si]/([Sn] + [Si]) ratio increases from 3 to 49 mol.%, there is a consistent increase in the intensity of oscillations of surface hydroxyl and silanol groups. However, in the spectrum of SnSi86 sample, a noticeable decrease in the intensity of vibrations of O–H and Si–OH bonds occurs. Perhaps this is due to the condensation reaction between the silanol and hydroxyl groups on the surface of SnO<sub>2</sub>:



This is due to the significantly larger number of formed SiO<sub>2</sub> particles. The spectra of SnSi3–SnSi19 samples contain the absorbance band at 960 cm<sup>−1</sup>, corresponding to the antisymmetric vibrations of the [SiO<sub>4</sub>] group associated with Sn<sup>4+</sup> (O<sub>3</sub>Si–Sn) [27]. The highest intensity of this absorption band is observed in the spectrum of the SnSi13 nanocomposite. This may correspond to the largest number of SiO<sub>2</sub> fragments formed on SnO<sub>2</sub> surface by heterogeneous nucleation. In the range of 700–400 cm<sup>−1</sup>, the spectra of composite samples contain all the absorption bands corresponding to the vibrations of the surface groups of individual SnO<sub>2</sub> and SiO<sub>2</sub>.

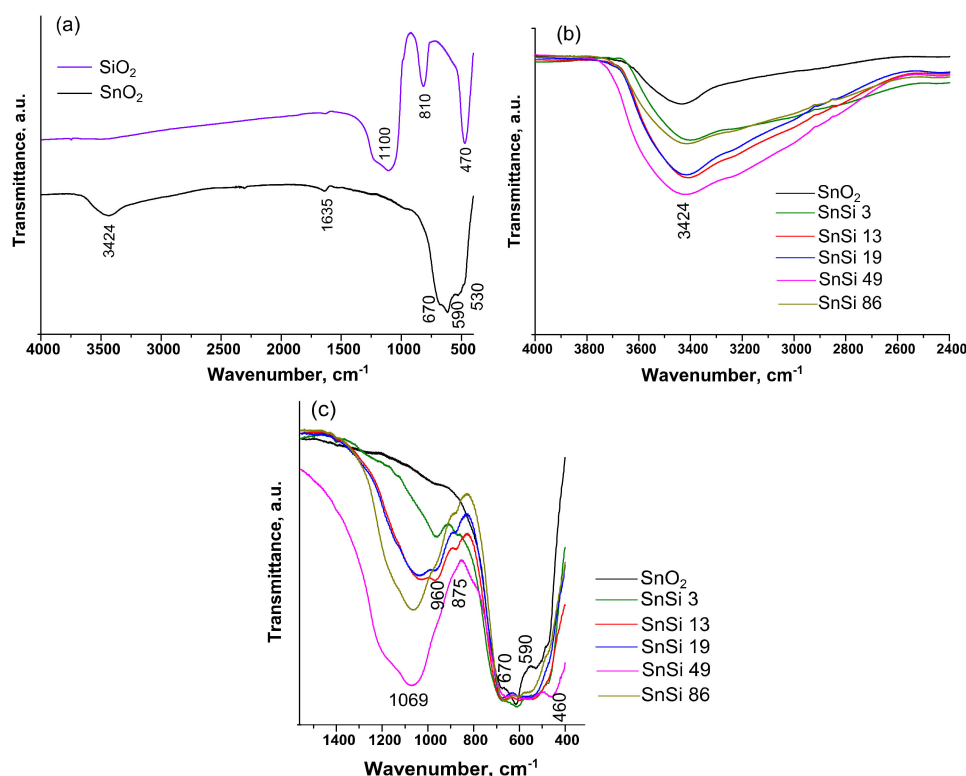
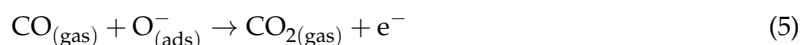
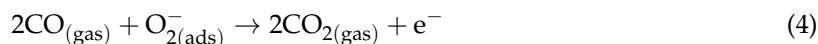


**Figure 7.** The IR spectra of the samples: (a) SnO<sub>2</sub> and SiO<sub>2</sub>; (b) SnO<sub>2</sub> and SnO<sub>2</sub>/SiO<sub>2</sub> with the ratio [Si]/([Sn] + [Si]) = 3, 13, 19, 49, and 86 mol.% in the range of 4000–2400 cm<sup>-1</sup> and (c) 1600–400 cm<sup>-1</sup>.

The main active groups on the SnO<sub>2</sub> surface involved in the redox reaction in the formation of a sensor signal are chemisorbed oxygen forms:



where CO<sub>(gas)</sub> is CO molecule in the gas phase, O<sub>2(ads)}</sub><sup>-</sup>, O<sub>(ads)}</sub><sup>-</sup> are different forms of chemisorbed oxygen, CO<sub>2(gas)</sub> is a product of the oxidation of CO gas desorbed into the gas phase. The change in concentration of chemisorbed oxygen in nanocomposites relative to unmodified SnO<sub>2</sub> was investigated by the XPS method. Figure 8 shows the survey X-ray photoelectron spectrum of the SnSi13 nanocomposite. The spectrum contains signals of C, O, Si, Sn. The presence of peak C1s (285.0 eV) related with residual carbon contamination on the surface of the samples associated with analysis preparation process. The positions of Sn3d<sub>5/2</sub> (486.6 eV) and Sn3d<sub>3/2</sub> (497.0 eV) peaks (Figure 9a) correspond to Sn(IV) in SnO<sub>2</sub> [28]. The spectrum in Si2p (Figure 9b) is described by a single component with an energy of 103.0 eV, corresponding to Si(IV) in SiO<sub>2</sub> [28]. For nanocrystalline SnO<sub>2</sub> and SnSi13 nanocomposite the XP-spectrum in O1s region has an asymmetrical shape and is described by two components (Figure 9c,d). The main peak (O1, E = 531.0 eV) corresponds to lattice oxygen in the structure of tin dioxide. The presence of a broad component with E = 532.1 eV (O2) is due to various forms of chemisorbed oxygen and hydroxyl groups. The ratio of the integral intensities of the components for pure SnO<sub>2</sub> is O2/O1 = 0.25. The introduction of SiO<sub>2</sub> leads to a significant increase in this value to O2/O1 = 0.36. This is consistent with the results obtained by IR spectroscopy, and may be due to an increase in the specific surface area.



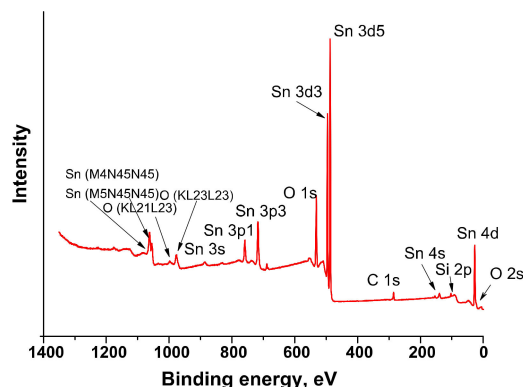


Figure 8. Survey X-ray photoelectron spectra of SnSi13 sample.

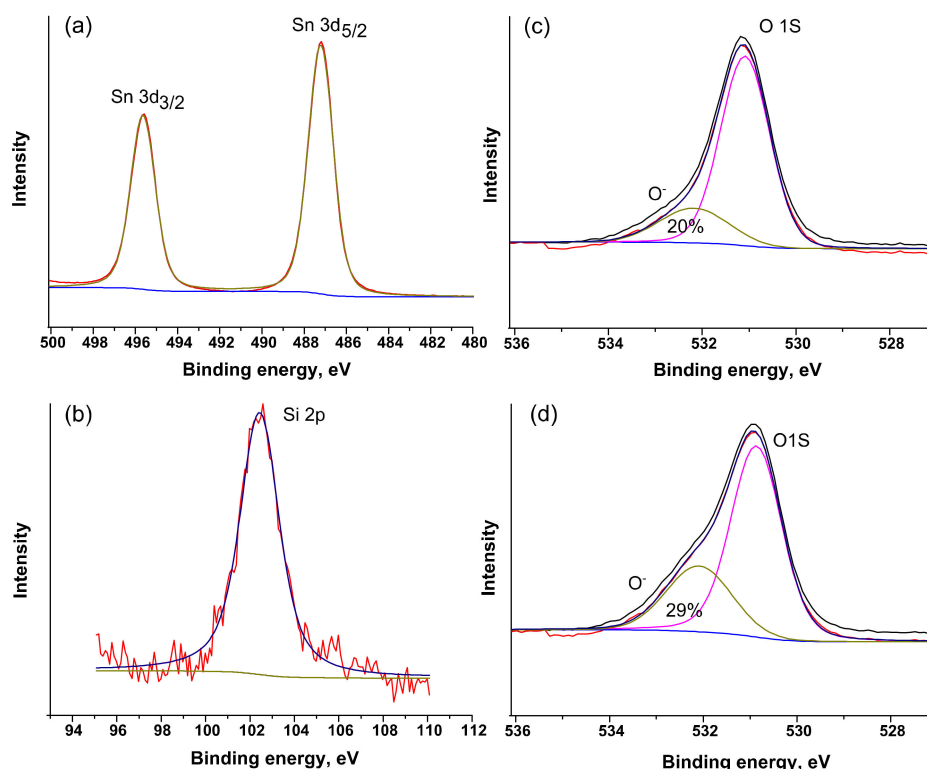
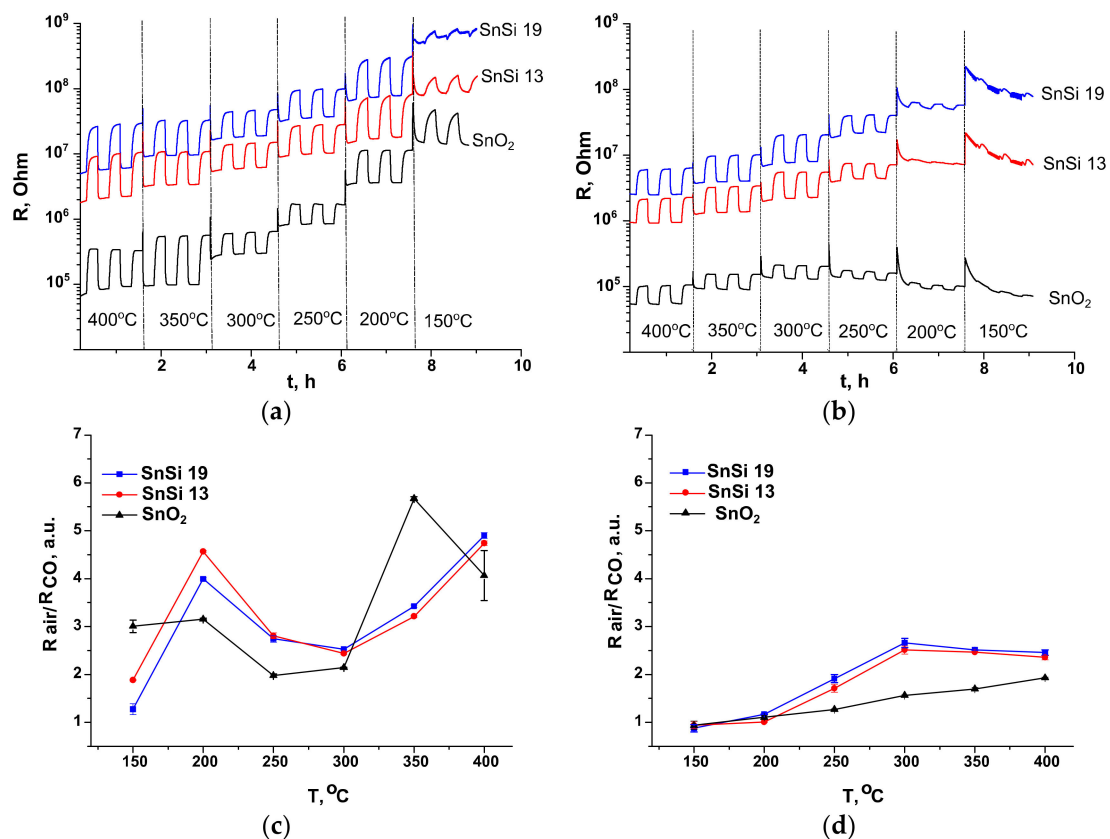


Figure 9. X-ray photoelectron spectra: (a) SnSi13 sample, Sn3d region; (b) SnSi13 sample, Si2p region; (c) SnO<sub>2</sub> sample, O1s region; (d) SnSi13 sample, O1s region.

Sensor properties of nanocrystalline SnO<sub>2</sub> and SnO<sub>2</sub>/SiO<sub>2</sub> nanocomposites toward CO were investigated by in situ conductivity measurements. Figure 10a,b shows the change in the resistance of SnO<sub>2</sub>, SnSi13 and SnSi19 samples with a periodic change in the composition of the gas phase in the presence of 100 ppm CO in dry air (RH = 1%) (Figure 10a) and at relative humidity RH = 20% (at 25 °C) (Figure 10b). Tin dioxide is n-type semiconductor, therefore when interacting with a reducing gas its resistance decreases in accordance with the Equations (4) and (5).

The sensor response of all measured samples (SnO<sub>2</sub>, SnSi13 and SnSi19) is well reproducible. On the temperature dependence of sensor response in dry air there are two maxima: at temperatures of 350 °C for SnO<sub>2</sub> and 400 °C for SnSi13, SnSi19, and also at 200 °C for all of the samples (Figure 10c). In humid air for nanocomposite samples, the maximum sensor response is observed at 300 °C, and in the case of pure tin dioxide, the magnitude of the response grows monotonically with increasing temperature up to 400 °C (Figure 10d). In general, an increase in air humidity leads to a decrease in the sensor response toward CO. However, for SnSi13 and SnSi19 nanocomposites at a measurement

temperature of 300 °C, the magnitude of the signal does not depend on air humidity. Based on these results, temperatures of 350, 300, and 200 °C were selected to build the calibration curves at RH = 1% and RH = 20%. For the indicated temperatures the values of sensor response were obtained at CO concentrations of 200, 100, 50, 20, and 10 ppm CO in humid and dry air. The dependences of the sensor response  $S$  on the concentration of carbon monoxide  $C_{CO}$  correspond to a power law  $S \sim C_{CO}^n$  and are linearized in double logarithmic coordinates (Figure 11).



**Figure 10.** Resistance of nanocrystalline SnO<sub>2</sub> and SnO<sub>2</sub>/SiO<sub>2</sub> nanocomposites in the temperature range 400–150 °C under the periodic change of the gas phase composition: (a) RH = 1%; (b) RH = 20%. Temperature dependences of the sensor response to 100 ppm CO in air: (c) RH = 1%; (d) RH = 20%.

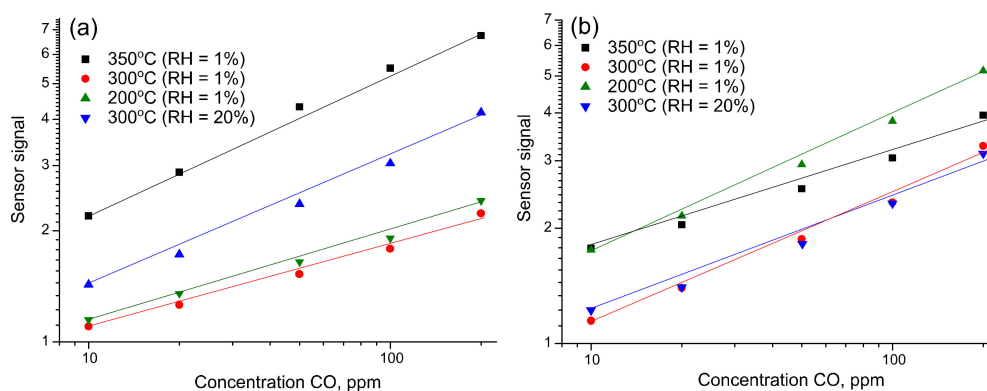


**Figure 11.** Cont.

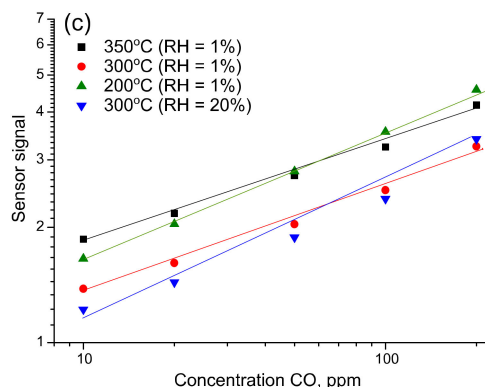


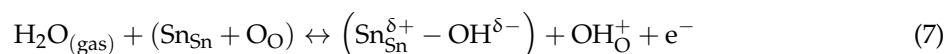
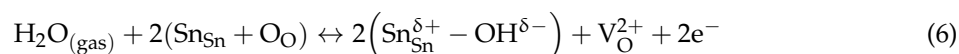
**Figure 11.** Calibration curves in double logarithmic coordinates for SnO<sub>2</sub> (a), SnSi13 (b) and SnSi19(c).

By calculating the average resistance value ( $R_{av}$ ) and the standard deviation ( $\sigma$ ) of resistance in air the values of detection limits (LDL), CO for each sensor was calculated from the obtained calibration curves. The value  $R_{av}/(R_{av}-3\sigma)$  was taken as the minimum measurable sensor signal. The results are presented in Table 2.

**Table 2.** CO detection limit (LDL) for SnO<sub>2</sub>, SnSi13 and SnSi19 samples, as well as the power coefficients ( $n$ ) calculated from obtained calibration curves.

Sample	RH = 1%				RH = 20%			
	350 °C		300 °C		200 °C		300 °C	
	$n$	LDL, ppm	$n$	LDL, ppm	$n$	LDL, ppm	$n$	LDL, ppm
SnO <sub>2</sub>	0.457 ± 0.007	1.5	0.20 ± 0.03	8.2	0.29 ± 0.02	6.9	0.21 ± 0.04	9.0
SnSi13	0.35 ± 0.02	4.3	0.31 ± 0.04	7.2	0.58 ± 0.05	3.0	0.34 ± 0.05	7.0
SnSi19	0.34 ± 0.02	3.3	0.30 ± 0.08	5.6	0.51 ± 0.04	2.4	0.29 ± 0.03	7.8

In humid air, the sensor's response decreases, and also the noise increases especially for the low temperature measurements (Figure 10b). However, SnO<sub>2</sub>/SiO<sub>2</sub> samples show greater sensor response as compared to pure SnO<sub>2</sub> (Figure 10d). The effect of humidity on the electrophysical properties of the samples was investigated by in situ conductivity measurements. The concentration of water vapor in the air with RH = 4%, 20%, and 65% (at 25 °C) is 0.031, 0.125, 0.625 and 2.032 vol.%, respectively. The decrease in sensor response toward CO in humid air can be explained by blocking of active centers on tin dioxide surface because of competitive adsorption of water molecules, which in turn result in the decrease in samples resistance due to the reactions:



So, one can calculate the value of the response to water vapor as  $S_{\text{RH}} = \frac{R_{\text{RH}=1\%}}{R_{\text{RH}}}$  (Figure 12). The measurements of sensor resistances in the temperature range of 400–100 °C showed that pure SnO<sub>2</sub> is the most sensitive to the content of water vapor in the air flow (Figure 12a). The response to water vapor of the SnSi13 sample (Figure 12b) over the all temperature range coincides in magnitude for all RH values, that indicates the stability of its characteristics under fluctuations in air humidity and the potential applicability of this material for CO detection in real conditions. The resistance of the SnSi19 sample varies less with increasing air humidity than pure tin dioxide (Figure 12c).

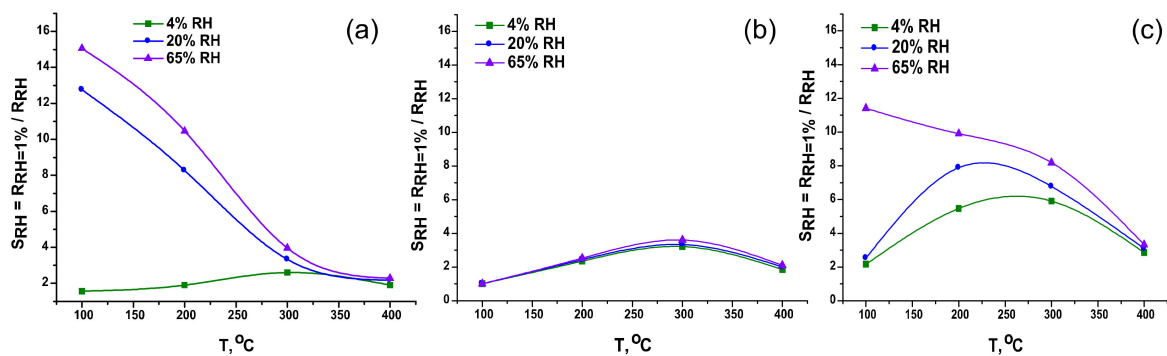


**Figure 12.** Temperature dependences of the response to water vapor of: (a) SnO<sub>2</sub>; (b) SnSi13; (c) SnSi19 at RH = 4, 20 and 65% (at 25 °C).

In humid air, the greater sensor response of SnO<sub>2</sub>/SiO<sub>2</sub> nanocomposites compared to pure SnO<sub>2</sub> may be due to the tolerance (reduced sensitivity) of their electrophysical properties to hydroxyl poisoning [15]. The main cause of this effect, in our opinion, is the predominant adsorption of water molecules on the surface of SiO<sub>2</sub> fragments. These fragments can act as moisture concentrators reducing hydroxyl poisoning for SnO<sub>2</sub> surface, which, in its turn, is responsible for the formation of the sensor response of nanocomposites.

The mechanism for improving the sensor characteristics of SnO<sub>2</sub>/SiO<sub>2</sub> nanocomposites compared to pure SnO<sub>2</sub> in humid air can be represented as follows (Figure 13). The SnO<sub>2</sub>/SiO<sub>2</sub> nanocomposites contain fragments of amorphous SiO<sub>2</sub>, which form an interface with the SnO<sub>2</sub> nanocrystals. In wet conditions, the adsorption of water vapor takes place predominantly on these SiO<sub>2</sub> fragments. This reduces the number of water molecules that are adsorbed on the surface of SnO<sub>2</sub>. As a result, the blocking of active centers on the tin dioxide surface, which causes a decrease in the sensor signal to CO in humid air, occurs to a lesser extent. This leads to the retention of a high sensor response to CO when the sensor is operating in humid air. The sensor based on the SnSi13 nanocomposite demonstrated the greatest indifference of the sensor response to changes in air humidity.

The set of the obtained results allows us to conclude that during the synthesis of the SnSi13 nanocomposite, an optimal supersaturation of the silica precursor was created, which ensured the formation of the maximum number of SiO<sub>2</sub> fragments on the SnO<sub>2</sub> surface through heterogeneous nucleation. This led to the formation of such a microstructure of the nanocomposite, which allowed reducing its sensitivity to hydroxyl poisoning and increasing the sensor response to carbon monoxide in humid air.

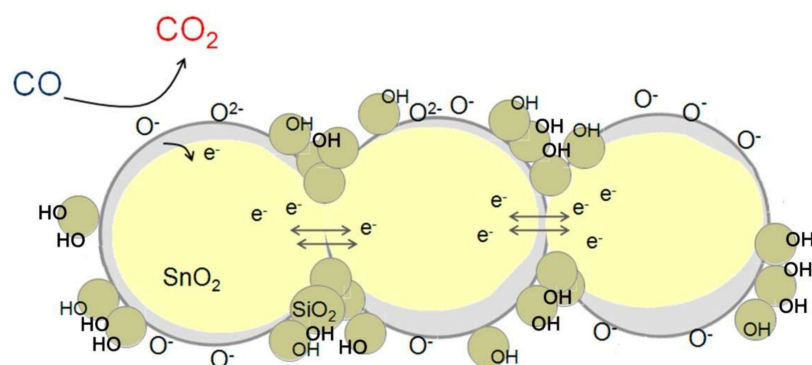


**Figure 13.** Schematic representation of the process of CO oxidation on the surface of SnO<sub>2</sub>/SiO<sub>2</sub> nanocomposite under wet conditions.

#### 4. Conclusions

SnO<sub>2</sub>/SiO<sub>2</sub> samples were synthesized with the ratio [Si]/([Sn] + [Si]) = 0, 3, 13, 19, 49, 86, and 100 mol.%. It is shown that the addition of SiO<sub>2</sub> in the range of [Si]/([Sn] + [Si]) = 3–19 mol.% allows the acquisition of materials with a high specific surface area during high-temperature annealing (600 °C) for 24h. The excess of indicated content of the dielectric in SnO<sub>2</sub>/SiO<sub>2</sub> composition leads to an increase in the sample's resistance above the critical value for sensor measurements. Characterization of composite materials by a complex of physicochemical methods showed that the addition of SiO<sub>2</sub> at the stage of hydrothermal treatment affects not only the microstructure of the obtained samples, but also changes the composition of surface-active groups, which alters the reactivity of the obtained materials. From FTIR data it can be supposed that SnO<sub>2</sub>/SiO<sub>2</sub> nanocomposite ([Si]/([Sn] + [Si]) = 13%) has the largest number of SiO<sub>2</sub> fragments formed on SnO<sub>2</sub> surface by heterogeneous nucleation. The sensor properties of SnO<sub>2</sub>/SiO<sub>2</sub> nanocomposites toward CO were investigated in dry (RH = 1%) and humid (RH = 20%) air in the temperature range 150–400 °C. It was observed that the magnitude of the sensor response of SnO<sub>2</sub>/SiO<sub>2</sub> nanocomposites at 300 °C does not depend on air humidity. When studying the effect of relative humidity in the range of RH = 4%–65%, it was found that the resistance of SnO<sub>2</sub>/SiO<sub>2</sub> nanocomposite ([Si]/([Sn] + [Si]) = 13%) is the least sensitive to the RH change over the whole range of operating temperatures. This may be due to its microstructure, which reduces its sensitivity to hydroxyl poisoning. The obtained results indicate the potential applicability of this material for CO detection in real conditions.

**Author Contributions:** Conceptualization, M.R. and A.G.; Methodology, D.G., M.R., A.M., and V.K.; Formal Analysis, D.G. and M.R.; Investigation, D.G., E.G., A.M., T.S., V.K. and N.K.; Data Curation, D.G. and M.R.; Writing—Original Draft Preparation, D.G. and M.R.; Writing—Review and Editing, M.R., E.G. and A.G.; Supervision, M.R.

**Funding:** This research was funded by the Russian Ministry of Education and Sciences (Agreement No. 14.613.21.0075, RFMEFI61317X0075).

**Acknowledgments:** The spectral research was carried out using the equipment purchased by funds of Lomonosov Moscow State University Program of the Development. The research by EDX was performed using the equipment of the Joint Research Center for Physical Methods of Research of Kurnakov Institute of General and Inorganic Chemistry of the Russian Academy of Sciences. Authors are grateful to Vadim Platonov and Alexey Yaprntsev for their assistance in EDX measurements.

**Conflicts of Interest:** The authors declare no conflict of interest.

#### References

1. Das, S.; Jayaraman, V. SnO<sub>2</sub>: A comprehensive review on structures and gas sensors. *Prog. Mater. Sci.* **2014**, *66*, 112–255. [[CrossRef](#)]
2. Martinelli, E.; Polese, D.; Catini, A. Self-adapted temperature modulation in metal-oxide semiconductor gas sensors. *Sens. Actuators B* **2012**, *161*, 534–541. [[CrossRef](#)]
3. Fonollosa, J.; Rodriguez-Luján, I.; Trincavelli, M.; Vergara, A.; Huerta, R. Chemical discrimination in turbulent gas mixtures with MO<sub>x</sub> sensors validated by gas chromatography-mass spectrometry. *Sensors* **2014**, *14*, 19336–19353. [[CrossRef](#)] [[PubMed](#)]
4. Rogers, P.H.; Benkstein, K.D.; Semancik, S. Machine learning applied to chemical analysis: Sensing multiple biomarkers in simulated breath using a temperature-pulsed electronic-nose. *Anal. Chem.* **2012**, *84*, 9774–9781. [[CrossRef](#)] [[PubMed](#)]
5. Illyaskutty, N.; Knoblauch, J.; Schwotzer, M.; Kohler, H. Thermally modulated multi sensor arrays of SnO<sub>2</sub>/additive/electrode combinations for enhanced gas identification. *Sens. Actuators B* **2015**, *217*, 2–12. [[CrossRef](#)]
6. Kovalenko, V.V.; Zhukova, A.A.; Rumyantseva, M.N.; Gaskov, A.M.; Yushchenko, V.V.; Ivanova, I.I.; Pagnier, T. Surface chemistry of nanocrystalline SnO<sub>2</sub>: Effect of thermal treatment and additives. *Sens. Actuators B* **2007**, *126*, 52–55. [[CrossRef](#)]
7. Toledo-Antonio, J.A.; Gutierrez-Baez, R.; Sebastian, P.J.; Vazquez, A. Thermal stability and structural deformation of rutile SnO<sub>2</sub> nanoparticles. *J. Solid State Chem.* **2003**, *174*, 241–248. [[CrossRef](#)]

8. Rac, O.; Suchorska-Woźniak, P.; Fiedot, M.; Teterycz, H. Influence of stabilising agents and pH on the size of SnO<sub>2</sub> nanoparticles. *Beilstein J. Nanotechnol.* **2014**, *5*, 2192–2201. [[CrossRef](#)]
9. Rozenberg, B.A.; Tenne, R. Polymer-assisted fabrication of nanoparticles and nanocomposites. *Prog. Pol. Sci.* **2008**, *33*, 40–112. [[CrossRef](#)]
10. Xu, C.; Tamaki, J.; Miura, N.; Yamazoe, N. Stabilization of SnO<sub>2</sub> ultrafine particles by additives. *J. Mater. Sci.* **1992**, *27*, 963–971. [[CrossRef](#)]
11. Hong, S.-J.; Han, J.-I. Improvement in the long-term stability of SnO<sub>2</sub> nanoparticle surface modification with additives. *J. Korean Phys. Soc.* **2006**, *48*, 1390–1394.
12. Chang, C.-H.; Gong, M.; Dey, S.; Liu, F.; Castro, R.H.R. Thermodynamic stability of SnO<sub>2</sub> nanoparticles: The role of interface energies and dopants. *J. Phys. Chem. C* **2015**, *119*, 6389–6397. [[CrossRef](#)]
13. Ross, J.R.H. *Contemporary Catalysis: Fundamentals and Current Applications*; Elsevier: Amsterdam, The Netherlands, 2018; p. 96.
14. Tricoli, A.; Graf, M.; Pratsinis, S.E. Optimal doping for enhanced SnO<sub>2</sub> sensitivity and thermal stability. *Adv. Func. Mater.* **2008**, *18*, 1969–1976. [[CrossRef](#)]
15. Gunji, S.; Jukei, M.; Shimotsuna, Y.; Miura, K.; Suematsu, K.; Watanabe, K.; Shimanoe, K. Unexpected gas sensing property of SiO<sub>2</sub>/SnO<sub>2</sub> core-shell nanofibers in dry and humid conditions. *J. Mater. Chem. C* **2017**, *5*, 6369–6376. [[CrossRef](#)]
16. Liu, Y.; Yang, P.; Li, J.; Matras-Postolek, K.; Yue, Y.; Huang, B. Formation of SiO<sub>2</sub>@SnO<sub>2</sub> core-shell nanofibers and their gas sensing properties. *RSC Adv.* **2016**, *6*, 13371–13376. [[CrossRef](#)]
17. Zhu, J.; Tay, B.Y.; Ma, J. Synthesis and mechanism study of mesoporous SnO<sub>2</sub>/SiO<sub>2</sub> composites. *J. Nanosci. Nanotechnol.* **2006**, *6*, 2046–2055. [[CrossRef](#)]
18. Zhan, Z.; Chen, J.; Guan, S.; Si, L.; Zhang, P. Highly sensitive and thermal stable CO gas sensor based on SnO<sub>2</sub> modified by SiO<sub>2</sub>. *J. Nanosci. Nanotechnol.* **2013**, *13*, 1507–1510. [[CrossRef](#)]
19. Asgari, M.; Saboor, F.H.; Mortazavi, Y.; Khodadadi, A.A. SnO<sub>2</sub> decorated SiO<sub>2</sub> chemical sensors: Enhanced sensing performance toward ethanol and acetone. *Mater. Sci. Semicond. Process.* **2017**, *68*, 87–96. [[CrossRef](#)]
20. Sun, Y.; Wang, J.; Li, X.; Du, H.; Huang, Q.; Wang, X. The effect of zeolite composition and grain size on gas sensing properties of SnO<sub>2</sub>/zeolite sensor. *Sensors* **2018**, *18*, 390. [[CrossRef](#)]
21. Nalimova, S.S.; Myakin, S.V.; Moshnikov, V.A. Controlling surface functional composition and improving the gas-sensing properties of metal oxide sensors by electron beam processing. *Glass Phys. Chem.* **2016**, *42*, 597–601. [[CrossRef](#)]
22. Gulevich, D.G.; Marikutsa, A.V.; Rumyantseva, M.N.; Fabrichnyi, P.B.; Shatalova, T.B.; Gaskov, A.M. Detection of carbon monoxide in humid air with double-layered structures based on semiconducting metal oxides and silicalite. *Russ. J. Appl. Chem.* **2018**, *91*, 1671–1679. [[CrossRef](#)]
23. Miodownik, M.; Holm, E.A.; Hassold, G.N. Highly parallel computer simulation of particle pinning: Zener vindicated. *Scr. Mater.* **2000**, *42*, 1173–1177. [[CrossRef](#)]
24. Rumyantseva, M.N.; Gaskov, A.M.; Rosman, N.; Pagnier, T.; Morante, J.R. Raman surface vibration modes in nanocrystalline SnO<sub>2</sub>: Correlation with gas sensor performances. *Chem. Mater.* **2005**, *17*, 893–901. [[CrossRef](#)]
25. Nakamoto, K. *Infrared and Raman Spectra of Inorganic and Coordination Compounds*; Wiley: Hoboken, NJ, USA, 1997.
26. Ferreira, C.S.; Santos, P.L.; Bonacin, J.A.; Passos, R.R.; Pocrifka, L.A. Rice husk reuse in the preparation of SnO<sub>2</sub>/SiO<sub>2</sub> nanocomposite. *Mater. Res.* **2015**, *18*, 639–643. [[CrossRef](#)]
27. Hwang, Y.K.; Jin, T.H.; Kim, J.M.; Kwon, Y.-U.; Park, S.-E.; Chang, J.-S. Microwave synthesis of metallosilicate zeolites with fibrous morphology. *J. Nanosci. Nanotech.* **2006**, *6*, 1786–1791. [[CrossRef](#)]
28. Thermo Scientific XPS Simplified. Available online: <https://xpssimplified.com/elements> (accessed on 1 March 2019).

